Mapping fracture networks at the microscale in concrete weight coatings for pipelines

Jiazheng Hu, Dept. of Civil & Mineral Engineering, University of Toronto, 35 St. George St., Toronto, Ontario, M5S 1A4, Canada,, jeremy.hu@mail.utoronto.ca

Ekaterina Ossetchkina, Dept. of Civil & Mineral Engineering, University of Toronto, 35 St. George St., Toronto, Ontario, M5S 1A4, Canada, ekaterina.ossetchkina@mail.utoronto.ca

Yusheng Qiu, Dept. of Civil & Mineral Engineering, University of Toronto, 35 St. George St., Toronto, Ontario, M5S 1A4, Canada, yusheng.qiu@mail.utoronto.ca

Karl Peterson, Dept. of Civil & Mineral Engineering, University of Toronto, 35 St. George St., Toronto, Ontario, M5S 1A4, Canada, karl.peterson@utoronto.ca

Giovanni Grasselli, Dept. of Civil & Mineral Engineering, University of Toronto, 35 St. George St., Toronto, Ontario, M5S 1A4, Canada, giovanni.grasselli@utoronto.ca

Sanjay Shah, Concrete - Research and Development, Shawcor, 25 Bethridge Rd, Etobicoke, Ontario, M9W 1M7, Canada

INTRODUCTION

Models of concrete performance at the operational scale often treat concrete as a homogeneous continuum, although heterogeneities present in the micro and mesostructure do affect the macroscopic behavior, especially crack initiation and propagation [1]. Fractures initiate through a series of complicated micromechanical processes, and can eventually coalesce and grow into macro-scale cracks. This research program begins with a forensic investigation of cylinders failed in compression, as a starting point to better understand the potential for fracture in concrete weight coatings (CWC) during pipeline placement and service. Microscopy plays an important role by mapping out cracks and phase locations (aggregate, paste, entrapped air voids) to inform mesh development for subsequent modeling. Initially, X-ray micro computed tomography (μCT) was employed on CWC cores, both before and after compression testing. For μCT, the resolution achieved is a function of the scanned volume; the larger the sample, the larger the voxel size. Given the core dimensions (Ø 38 mm, 60 mm length) a voxel size of 72 μm^3 was achieved with the GE V|tome|x|240D μCT. The density contrast between the heavyweight iron ore and iron nickel slag aggregates, the hydrated paste, and air voids allowed for easy phase distinction, but the resolution was not sufficient to resolve narrow crack planes. As an alternative the cores were stabilized with fluorescent epoxy, cut into slabs, and the surfaces characterized using a combination of x-ray micro fluorescence (μXRF) and optical fluorescence images, to generate the 2D images used for mesh development.

EXPERIMENTAL

Stabilization

A combined low-pressure/high-pressure fluorescent epoxy stabilization procedure was employed [2]. First, cores were stacked and placed in a 0.1 mm thickness low density polyethylene (LDPE) sleeve that was sealed at the bottom, but open at the top. Next, the sleeve was placed in a vacuum chamber, and subjected to low vacuum (10 KPa) conditions for 30 minutes, after which fluorescent epoxy was allowed into the chamber through flexible LDPE tubing so as to fill the sleeve and cover the cores. Next, the chamber was vented, the sleeve removed, and an overhand knot tied using the excess sleeve length, while taking care to squeeze out any air bubbles trapped in the liquid epoxy resin. The sealed sleeve was placed in a pressure chamber, and hydrostatically pressurized to 25 MPa, forcing the epoxy into any remaining unsaturated cracks and pores.

Characterization

After the epoxy had hardened, the cores were cut longitudinally into ~8 mm thick slabs. A 3*8 mosaic of overlapping 1392*1049 pixel images were recorded from each slab face using a Nikon SMZ-2T stereo zoom microscope equipped with a Luminera INFINITY 2 CCD camera, a UV ring illuminator, and a mechanical xy stage. The images were stitched together in Fiji to yield a single 17.8 μm pixel resolution image covering the entire face (Figure 1a) [3,4].

Characteristic Kα X-ray elemental maps (Si, Ca, K, Fe) were collected from the same faces using a Bruker M4 Tornado μXRF equipped with a Rh target, a poly-capillary lens with spot size of Ø50 μm, and a 30 mm^2 silicon drift detector (SDD). Elemental maps were collected at an accelerating voltage of 40 kV, a current of 200 μA, a 50 μm step size, with a 12 ms dwell time (Figure 1b). The elemental maps were used to perform a supervised classification in MultiSpec [5] for Fe-rich (hematite) Si-rich (chert) and K-rich (feldspar) aggregate, as well as cement paste and void space. The final classified phase image was aligned with the fluorescent image in Fiji [3,6] and the images combined to yield the final image used as the basis for mesh generation (Figure 2).

Image-based meshing for numerical simulation

Thanks to rapid increases in computational power, and recent developments in image processing techniques, researchers can generate model meshes that more realistically represent the internal structure of concrete [7]. Commercial software packages as well as free utilities developed by researchers are available to generate mesh based on the real structure [8,9]. However, these are often run in an isolated stand-alone package, or not scalable for more general purpose.

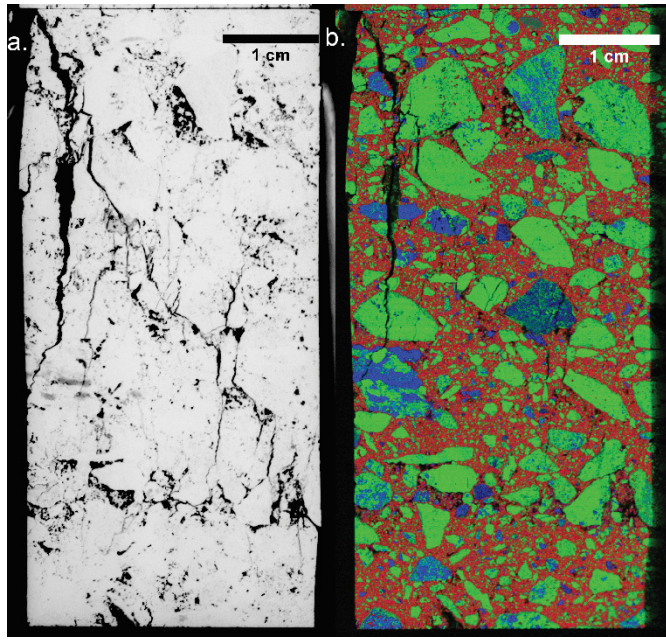

Figure 1: (a) inverted stereomicroscope UV image; (b) Ca-Fe-Si RGB μXRF elemental map.

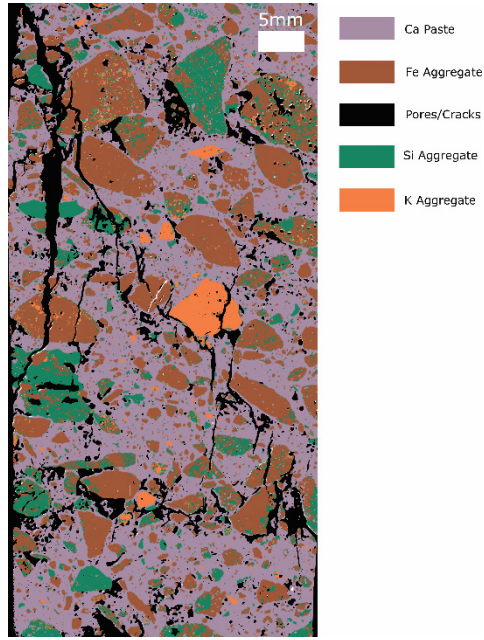

Figure 2: Classified phase image used for mesh input.

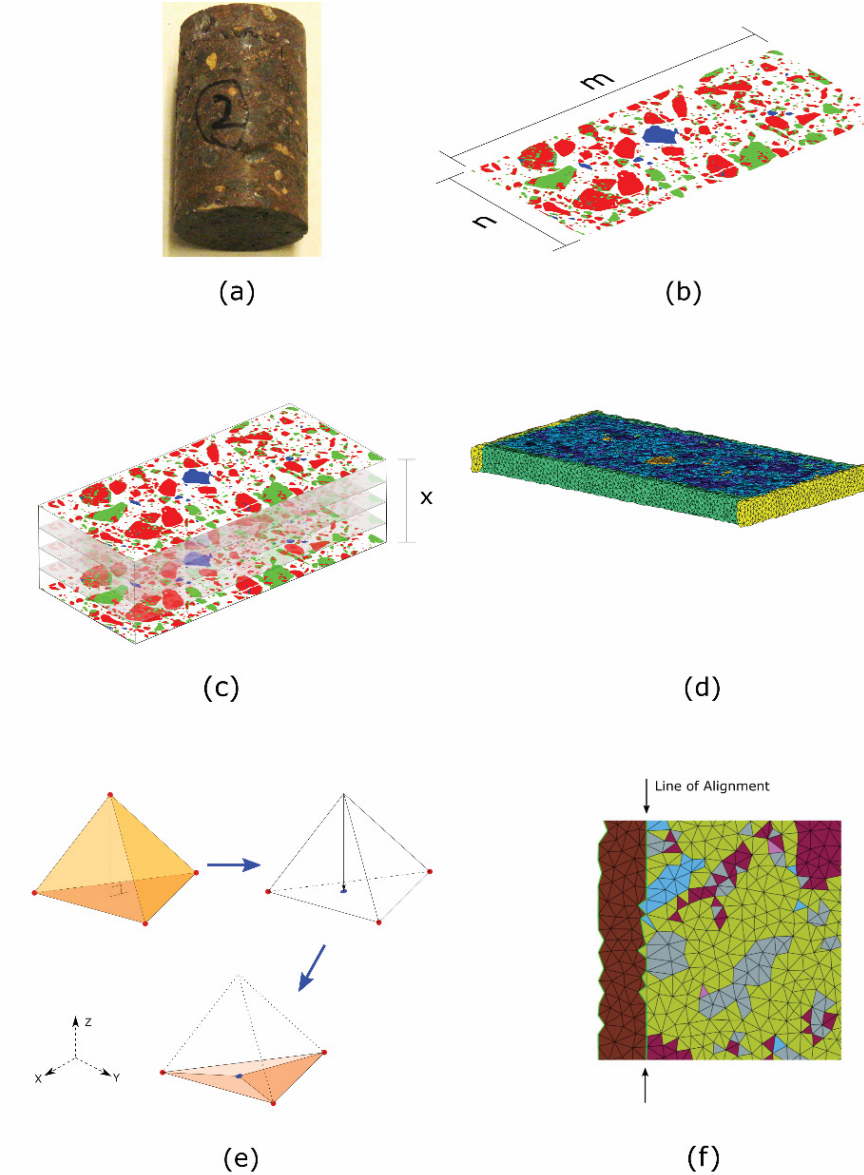

Figure 3: Approach for image-based meshing. (a) concrete cylinder slabbed for UV imaging and μXRF elemental mapping (b) classified phase image from slab surface; (c) self-stacked volumetric image; (d) tetrahedral mesh generated by ISO2MESH utility; (e) nodal projection mechanism to form final 2D mesh; (f) localized mesh modification along concrete exterior.

The 2D image-based mesh generation technique employed here was accomplished in MATLAB®. Using Figure 2 as the input, rectangles representing the steel platens were added, and the resulting 2D image was stacked to form a volume (Figure 3c). The volume was then meshed with tetrahedral elements using ISO2MESH (Figure 3d) [10]. Finally, the tetrahedral vertices were projected to the base (Figure 3e) to provide the basis for the 2D surface mesh (Figure 3f). Further adjustments to the 2D mesh were applied in an effort to smooth the edges of the concrete, and the contact between theplaten and the concrete. This was accomplished by re-classifying triangles that protruded from the concrete as either empty space (along edge) or as part of the steel platen (along platen/concrete contact) to yield the final 2D mesh image (Figure 4).

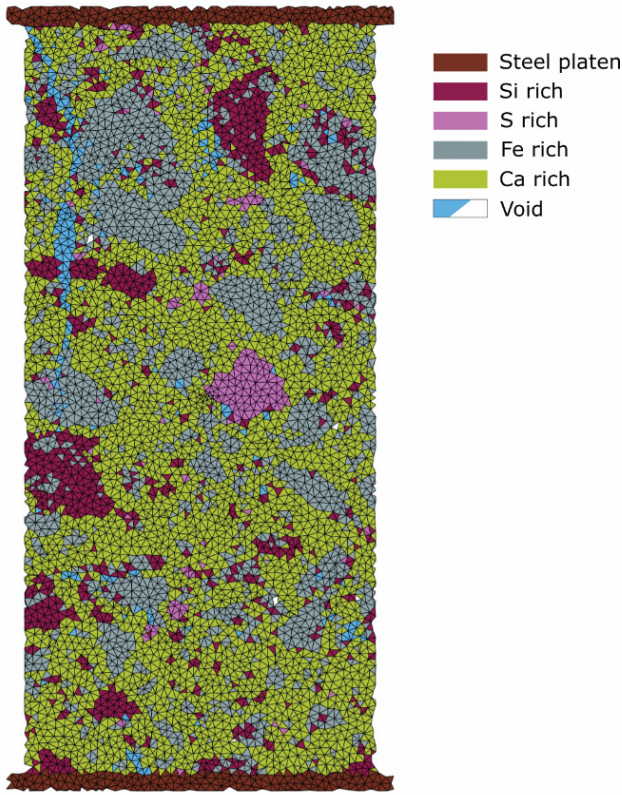

Figure 4: Sample final mesh.

CONCLUSIONS

A feasible approach for 2D mesh generation based on microscopic images collected from a cross-section through a concrete core is presented. Tetrahedra representing crack void space still need to be reclassified as either paste or aggregate, depending on

the identities of the surrounding tetrahedral, in order to represent the core prior to compressive strength testing. Another area with room for improvement is the artificial roughness introduced along aggregate/paste boundaries, and along the exterior boundaries of the concrete. An alternative outline-based approach may better deal with this issue.

ACKNOWLEDGEMENTS

We acknowledge the support of Shawcor, and the Natural Sciences and Engineering Research Council of Canada (NSERC) Collaborative Research and Development (CRD) and Ontario Centres of Excellence (OCE) Voucher for Innovation and Productivity (VIP II) grant programs.

REFERENCES

[1] Rodrigues E.A., Manzoli O.L., Bitencourt Jr., L.A.G., Bittencourt T.N. (2016) "2D mesoscale model for concrete based on the use of interface element with a high aspect ratio" *International Journal of Solids and Structures*, 94-95, 112–124. doi:10.1016/j.ijsolstr.2016.05.004.

[2] Laugesen P. (2012) Personal commincation, Pelcon Materials & Testing ApS.

[3] Schindelin J., Arganda-Carreras I., Frise E., Kaynig V., Longair M., Pietzsch T., Preibisch S., Rueden C., Saalfeld S., Schmid B., Tinevez J. Y., White D. J., Hartenstein V., Eliceiri K., Tomancak P., Cardona A. (2012) "Fiji: an open-source platform for biological-image analysis," *Nat Methods*, 9(7), 676-682, doi:10.1038/nmeth.2019

[4] Preibisch S., Saalfeld S., Tomancak P., (2009) "Globally optimal stitching of tiled 3D microscopic image acquisitions," *Bioinformatics*, 25(11), 1463–1465, doi: 10.1093/bioinformatics/btp184.

[5] Biehl L., Landgrebe D. (2002) "MultiSpec—a tool for multispectral–hyperspectral image data analysis" *Computers & Geosciences*, 28(10), 1153-1159. doi:10.1016/S0098-3004(02)00033-X

[6] Arganda-Carreras I., Sorzano C.O.S., Marabini R., Carazo J.-M., Ortiz-de Solorzano C., Kybic J. (2006) "Consistent and Elastic Registration of Histological Sections using Vector-Spline Regularization," Lecture Notes in Computer Science, Springer Berlin / Heidelberg, volume 4241/2006, CVAMIA: Computer Vision Approaches to Medical Image Analysis, 85-95.

[7] Coleri E., Harvey J.T.; Yang K., Boone J.M. (2013*)* "Investigation of asphalt concrete rutting mechanisms by X-ray computed tomography imaging and micromechanical finite element modeling" *Mater Struct*, 46 (6), 1027–1043. doi: 10.1617/s11527-012-9951-x

[8] Jivkov, A.P., Engelberg D.L.; Stein R., Petkovski M. (2013), "Pore space and brittle damage evolution in concrete" *Engineering Fracture Mechanics*, 110, 378–395. doi:10.1016/j.engfracmech.2013.05.007

[9] Huang Y., Yang Z., Ren W., Liu G., Zhang C. (2015) "3D meso-scale fracture modelling and validation of concrete based on in-situ X-ray Computed Tomography

images using damage plasticity model"*International Journal of Solids and Structures*, 67-68, 340–352. doi:10.1016/j.ijsolstr.2015.05.002
[10] Fang Q., Boas D. (2009) "Tetrahedral mesh generation from volumetric binary and gray-scale images" *Proceedings of IEEE International Symposium on Biomedical Imaging*, 1142-1145.